PCCP

COMMUNICATION

$Mn_2@Si_{15}$: the smallest triple ring tubular silicon cluster†

Hung Tan Pham,[a] Thu-Thuy Phan,[a] Nguyen Minh Tam,[ab] Long Van Duong,[a] My Phuong Pham-Ho[a] and Minh Tho Nguyen*[b]

Cite this: *Phys. Chem. Chem. Phys.*, 2015, **17**, 17566

Received 18th April 2015,
Accepted 9th June 2015

DOI: 10.1039/c5cp02257f

www.rsc.org/pccp

The smallest triple ring tubular silicon cluster $Mn_2@Si_{15}$ is reported for the first time. Theoretical structural identification shows that the $Mn_2@Si_{15}$ tubular structure whose triple ring is composed by three five-membered Si rings in anti-prism motif, is stable in high symmetry (D_{5h}) and singlet ground state ($^1A_1'$). The dimer Mn_2 is placed inside the tubular along the C_5 axis, and the Mn dopant form single Si–Mn bonds with Si skeleton, whereas the Mn–Mn is characterized as a triple bond. The effect of Mn_2 on the stability of the Si_{15} triple ring structure arises from strong orbital overlap of Mn_2 with Si_{15}.

Introduction

The element of silicon plays an essential role in the current electronic, optical and semiconductor industries.[1,2] These applications led to careful investigations on the chemical and physical properties of nano-scale silicon-based materials. In particular, geometric and electronic structures, as well as thermodynamic and spectroscopic properties of silicon clusters have extensively been explored in the last decades.[3–12] In the search for materials with tailored properties, the use of impurities, or dopants, is considered as an efficient approach. The presence of dopants invariably changes the geometric and electronic features, subsequently giving new properties such as higher thermodynamic stabilities, higher catalytic activities,[13] and quenched spin state. Within aim of finding for assembled nanomaterials, pentagon-based silicon clusters can server as unit for formation of Si wires,[14,15] a doping of transition metal atoms usually leads to formation of high symmetry cages with enhanced stability which are potential building-units.[16–18]

Following an earlier establishment of transition metal doped silicon clusters in which endohedral-like structures were identified to be the most stable doped derivatives,[19] a large number of systematic studies on doped silicon clusters Si_nM, with metal and non-metal dopants M were reported. Metal encapsulated silicon cages were found to be favoured usually starting from the size $n \geq 12$. The high thermodynamic stabilities of doped silicon clusters Si_nM result from strong overlap of d-AOs(M) and sp-AOs(Si atoms), and consequently give rise to a molecular orbital pattern which satisfies the electron shell model, or the 18 electrons rule of transition metal complexes. A typical example for the electron shell model on transition metal doped silicon clusters is the case of the $Mn@Si_{14}^+$ cation.[20] This endohedrally doped fullerene exhibits a completely quenched spin, and the shell of [2S, 2P, 2D] is fully occupied in its singlet ground state.

Following a similar doping strategy, the $M@Si_n^q$ doped-silicon clusters in various charged states, with M being Li, Be, B, V, Mn, Cu and Co were investigated,[21–23] and some interesting results include perhaps the boron-doped anion Si_9B^- and cation $Si_{10}B^+$ which attain the magic numbers with 40 and 42 electrons, respectively, and each contains 8 π-electrons thus obeying a spherical aromatic character. $Be@Si_8$ which has 34 itinerant electrons also completes the electron shell and present a case with a cubic aromatic character.[22]

The 18 electron counting rule which was previously applied to the $Cr@Si_{12}$ cluster,[24] but it was recently critically reexamined,[25] and accordingly, $Cr@Si_{12}$ does not exactly satisfy the 18 electrons count.

As far as we are aware, investigations of multiple metal atom doped silicon clusters are rather limited. The Mo_2Si_n clusters[26] and $M_2@Si_{18}$ with M = Ti–Zn,[27] and $V_3@Si_n$[28,29] were investigated to examine the effects of multiple metal doping. In view of the scarcity of reliable studies on multiply doped silicon clusters, we set out to carry out a systematic theoretical investigation on the doubly doped $M_2@Si_n$ in which M is a first-row transition metal atom. In this Communication, we wish to report a remarkable result showing a strong doping effect induced by

[a] *Institute for Computational Science and Technology (ICST), Ho Chi Minh City, Vietnam*

[b] *Department of Chemistry, KU Leuven, Celestijnenlaan 200F, B-3001 Leuven, Belgium. E-mail: minh.nguyen@chem.kuleuven.be*

† Electronic supplementary information (ESI) available: Comparison of MO shapes produced by DFT calculations with wavefunctions obtained by hollow cylinder model for the triple ring Si_{15} tubular form. See DOI: 10.1039/c5cp02257f

two manganese atom on the size of Si_{15}. While pure tubular silicon clusters are rather non-existent, we now find that $Mn_2@Si_{15}$ features a triple ring form in which the dimer Mn_2 is endohedrally incorporated at the centre of the tubular structure.

Electronic structure theory computations are carried out using the Gaussian 09 programs.[30] Equilibrium structures are identified using density functional theory (DFT). A careful calibration[20] of the performance of different DFT functionals for $Mn@Si_{14}^+$ pointed out that pure functionals such as the PBE and BP86 perform quite well for the singlet–triplet energy separation of the cation, as compared with the wavefunction CASPT2 method. Therefore, we select in the present work the BP86 functional for the search of $Mn_2@Si_{15}$ isomers. Possible structures are initially generated using a stochastic genetic search method.[31] Of the thousands structures generated, a selection of ~500 isomers were optimized using the BP86 functional in conjunction with the 3-21G(d) basis set. Lower-lying isomers within a range of 50 kcal mol^{-1} on relative energies, were then reoptimized using the BP86/6-311G(d) level. Finally the resulting lower-lying equilibrium structures are again reoptimized using the same functional but with the larger cc-pVTZ basis set.[32]

Structure of $Mn_2@Si_{15}$ clusters

Structural identification for the two Mn atoms doped Si_{15} cluster using BP86/cc-pVTZ optimizations is displayed in Fig. 1. Accordingly, the most stable isomer **I**, which is structurally characterized as a tubular form whose triple ring (TR) composed by three five-membered Si rings in an anti-prism motif, and the dopant Mn_2 dimer is placed inside the TR, is identified in a high symmetry D_{5h} and a singlet ground state $^1A_1'$. The shape, Mayer bond order (MBO) and bond length of **I** are depicted in Fig. 2. The triplet state counterpart of **I** kept the D_{5h} point group but it is 21 kcal mol^{-1} less stable than **I** (D_{5h}, $^1A_1'$). The next isomer **II** (C_1, ^1A) is however only 2 kcal mol^{-1} above **I**, while its high spin state (C_1, ^3A) is now 14 kcal mol^{-1} higher in energy. Isomer **II** results from a distortion of the TR **I**. The next isomer **III** is also found to have a TR, in both singlet (C_s, $^1A'$) and triplet (C_1, ^3A) states, but they are less stable, being 11 and 12 kcal mol^{-1} higher in energy than **I** (D_{5h}, $^1A_1'$), respectively. Both singlet and triplet fullerene forms **IV** (C_s, $^1A'$ and $^3A''$) are 18 and 10 kcal mol^{-1} above **I**, while both states of isomer **V** (C_1, ^1A) and (C_1, ^3A) are located at 14 and 18 kcal mol^{-1} above **I**. Within the expected accuracy of the DFT method employed here, both isomers **I** and **II** can be regarded as energetically degenerate.

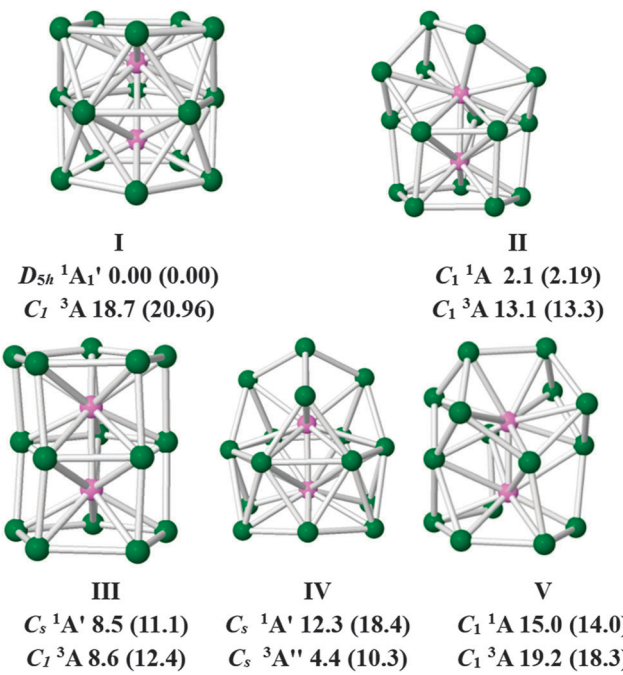

Fig. 1 Geometry and relative energy (kcal mol^{-1}) of the lower-lying isomers of $Mn_2@Si_{15}$ cluster. Energies were obtained at BP86/cc-pVTZ, (BP86/6-311G(d), values in parentheses), all with ZPE corrections.

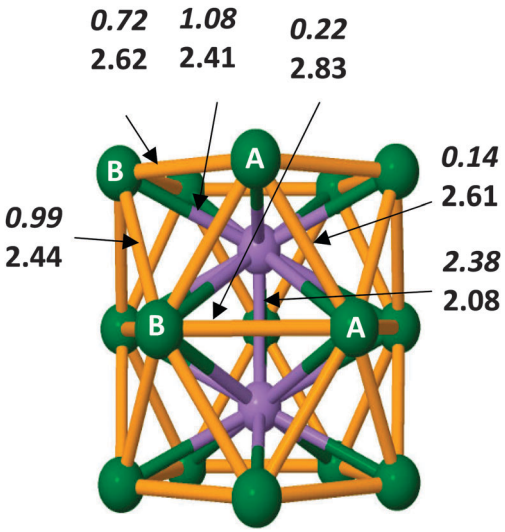

Fig. 2 Structural characteristics of the singlet $Mn_2@Si_{15}$ triple ring structure. Bond order: upper italic values, and bond length: lower values in angstrom (BP86/cc-pVTZ).

$Mn_2@Si_{15}$ **I** is thus discovered for the first time as a triple ring tubular form of doped silicon clusters. In fact, the singly doped $Si_{15}Mn$ exhibits a cage structure in which Mn is located inside Si_{15} cage.[33] The Sc, Ti and V dopants are found to favour a fullerene-like structure in which dopant is located at a central position as in Si_{16}.[34] $Si_{15}Fe$ appears in a fullerene-like form similar to $Si_{15}Mn$ cluster.[35] These results point out a different behaviour of two Mn dopants that significantly stabilize a Si_{15} triple ring shape.

Analysis of electronic structure

The electronic structure of the singlet $Mn_2@Si_{15}$ **I** is examined using the electron localizability indicator (ELI_D) approach,[36] which consists in a partition of the total electron density into basins where electrons are distributed. Fig. 3 shows the ELI_D maps for $Mn_2@Si_{15}$ plotted at the bifurcation values of 1.3 and 1.4. At value of 1.3, the iso-surface contours are split in to 15 localization domains corresponding to 15 Si cores. The V(Mn,Si) basins are observed only at smaller bifurcation values. However this does not imply that both Mn and Si atoms do not

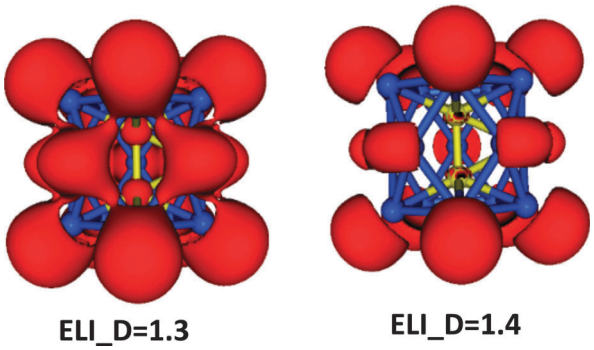

Fig. 3 The ELI_D maps of the triple ring $Mn_2@Si_{15}$ produced at the bifurcation values of 1.3 and 1.4 (BP86/6-311G(d)).

form direct chemical bonding (the radii of both Mn and Si atoms are large). More importantly, the distances between Mn and Si are relatively large, thus leading to small concentration of electron density.

As given in Fig. 2, the connection between the Mn atoms and Si skeleton is located on the first five-membered ring, noted as Si_1-A, B, which has a bond length of 2.41 Å and a MBO value of 1.1, which is consistent with an occupation number of 1.5 electrons obtained by separate NBO calculations. The Mn–Si_1 bonds can be considered as single character. The bond order for Mn–Si_2 bond has a value of 0.14, while the corresponding length amounts to 2.61 Å. Thus the Mn atom only weakly connects to Si_2 units. The bond length of the singlet Mn_2 dimer inside **I** is calculated at 2.08 Å (BP86), and the MBO for this bond is 2.38. This thus confers a triple bond character for the Mn–Mn bond. As given in Fig. 2, the Si–Si connections both in a ring and inter-rings are characterized as single bonds. Thus, the two Mn atoms connect with Si atoms through single Mn–Si bonds, while both Mn atoms makes a triple bond in a dimeric form.

The electron shell model

The transition metal doped clusters of IV elements, such as Si, Ge, Sn and Pb, lead to form the $M@E_{12}$ motif.[37–44] This kind of structure is also found in the Au,[45] and Ag[46] clusters with transition metal dopants. The high stability of singly doped $M@E_{12}$ was rationalized as a results of a strong stabilizing orbital interaction of metal atom with the E_{12} host giving rise to a MO pattern of $M@E_{12}$ satisfying the eigenstates produced by the shell model. The stability of the $Mn_2@Si_{15}$ ground state can also be examined using this simple approach. In the shell model, nuclei are ignored and replaced by a mean field while electrons are considered to move freely within this mean field. The valence electrons are filled the S, P, D, F,... orbitals according to the angular momentum number $L = 0, 1, 2, 3...$ With a given quantum number L, the lowest-lying level has a principle number $N = 1$. Within the shell model, the successive occupation of a level, giving a magic number, leads to a stabilized cluster.

Fig. 4 displays the partial densities of state (pDOS) calculated for Mn–Mn dimer and Si_{15} counterpart, respectively, and the total densities of state (DOS) that involve all contributions of both dopant Mn atoms and the Si_{15} host. Combining with

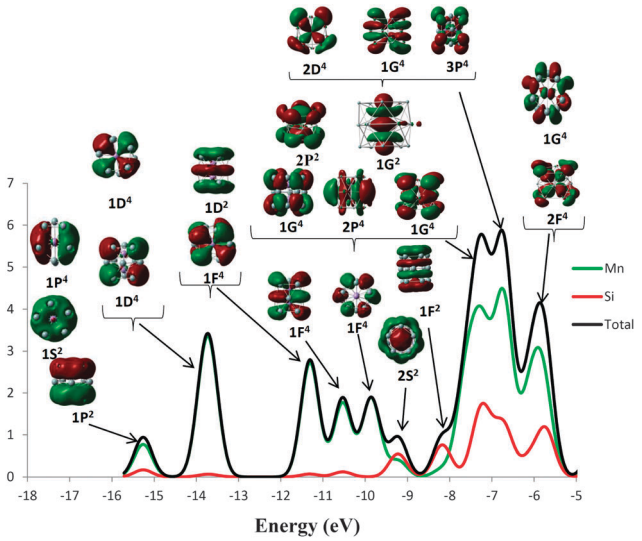

Fig. 4 Total (DOS) and partial (pDOS) densities of states of $Mn_2@Si_{15}$ **I**. The MOs obtained by BP86/6-311G(d) computations.

the shape of MOs, the electron shell configuration assigning for the $Mn_2@Si_{15}$ TR **I**, which includes a total number of 60 valence electrons, is identified as follows:

I: $[1S^2\ 1P^6\ 1D^{10}\ 1F^{12}\ 2S^2\ 1F^2\ 2P^6\ 1G^{10}\ 2D^4\ 1G^4\ 3P^4\ 1G^4\ 2F^4]$.

With the principle number $N = 1$, the sublevels S, P, D, F and G corresponding to the angular momentum number $L = 0, 1, 2, 3$ and 4 are fully occupied by 2, 6, 10, 14 and 18 electrons, respectively, whereas with $N = 2$, only subshells of 2S and 2P are fully filled by 2 and 6 electrons. The sublevels of 2D, 2F and 3P are each doubly degenerate, and occupied by 4 electrons for each level. The ground state of Mn_2Si_{15} **I** has a triple ring tubular shape which differs much from the spherical shape (as the standard shell model assuming electrons freely move in a spherical pseudopotential). Accordingly, the shells of G, F, D and P with $N = 1, 2$ and 3 are now split in to sublevels. Hence, the shell configuration of $Mn_2@Si_{15}$ tubular form can be considered as a successive occupation by 2, 6, 10, 14, 18, 2, 6, 4, 4, 4 electrons for 1S, 1P, 1D, 1F, 1G, 2S, 2P, 2D and 2F levels, respectively.

Orbital interaction diagrams

The model of a particle in hollow cylinder box (HCM) accounts successfully for the electronic structure of the B_{27}^+ triple ring boron tubular form in which delocalized MOs are classified in to three MO sets, namely core s-MOs, tangential t-MOs and radial r-MOs.[47,48] The MOs of the Si_{15} TR structure are basically reproduced by using this model. The eigenstates of Si_{15} triple ring form will be denoted as $(n\ k\ l)_x$ with n, k, l being quantum numbers and x = s, t, r stand for s-MOs, t-MOs and r-MOs sets. A comparison on MO shapes produced by DFT calculation and HCM model are shown in Fig. S1, S2 and S3 of ESI.† In a further attempt to understand the intrinsic stability of $Mn_2@Si_{15}$ TR **I**, orbital interaction diagrams of the Mn_2 dimer and Si_{15} TR are plotted in Fig. 5 and 6.

Fig. 5 depicts the interaction of frontier orbitals located on the Si_{15} triple ring structure with the MO of Mn_2 dimer that

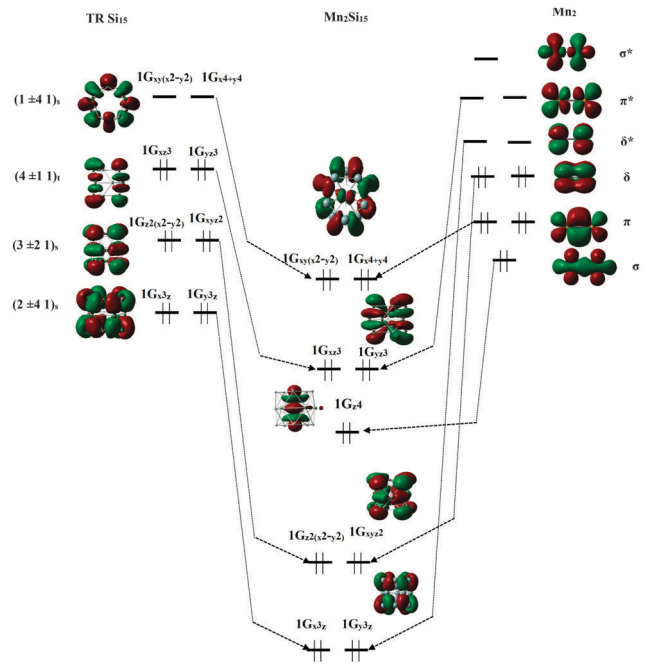

Fig. 5 An orbital interaction diagram of TR Si_{15} and Mn_2 which produces the 1G subshell of $Mn_2@Si_{15}$ **I** in terms of the shell model.

gives rise to the 1G sublevel. The anti-bonding π* MO of Mn_2 forms a stabilizing combination with the $(4\ \pm1\ 1)_t$ eigenstates of Si_{15} unit, turning out to be the $1G_{xz}{}^3$ and $1G_{yz}{}^3$ levels of $Mn_2@Si_{15}$ **I**. The two δ*-MOs are stabilized by interacting with $(2\ \pm4\ 1)_s$ levels of Si_{15} counterpart, finally producing the $1G_x{}^3{}_z$ and $1G_y{}^3{}_z$ subshells. The $1G_z{}^4$ level of **I** is basically established by contributions from the σ-MO of Mn_2 dimer.

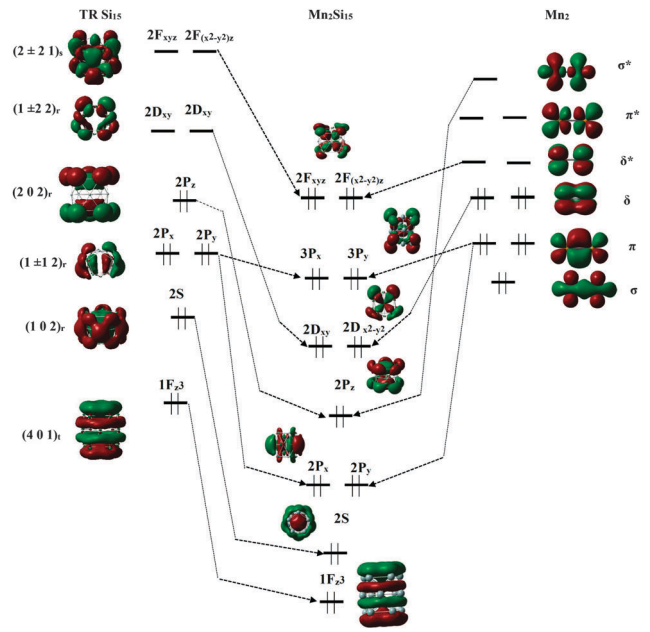

Fig. 6 An orbital interaction diagram of TR Si_{15} and Mn_2 which yields the 1F, 2P, 2D and 3P levels of $Mn_2@Si_{15}$ **I** in terms of the shell model.

Although the $1G_{xy(x^2-y^2)}$ and $1G_{x^4+y^4}$ subshells are formed by overlapping π-MOs of Mn_2 with empty $(1\ \pm4\ 1)_s$ levels of Si_{15}, these sublevels mainly have the characteristics of $1G_{xy(x^2-y^2)}$ and $1G_{x^4+y^4}$ MOs.

As given in the Fig. 6, the stability of δ bond is also enhanced by strong overlap with $(1\ \pm2\ 2)_r$ and $(3\ \pm2\ 1)_s$ solutions of Si_{15} TR yielding the pairs $2D_{xy}$ and $2D_{(x^2-y^2)}$ and $1G_z2_{(x^2-y^2)}$ and $1G_{xyz}2$ of the corresponding subshells of Mn_2Si_{15}. As illustrated in Fig. 6, the π-MOs gain an extra stability due to an interaction to the P_x and P_y MOs, which correspond to the $(1\ \pm1\ 2)_r$ of Si_{15} TR (not only the $2P_x$ and $2P_y$ but also $3P_x$ and $3P_y$ MOs). For their part, the δ*-MOs are stabilized by a stabilizing interaction to $2F_{xyz}$ and $2F_{(x^2\ -\ y^2)}$ assigning as $(2\ \pm2\ 1)$s levels in term of the HCM, generating the same sublevels of I. The σ*-MO which is high energy, forms a stabilizing overlap with the $(2\ 0\ 2)_r$ MO of Si_{15} TR resulting in the $2P_z$ subshell for Mn_2Si_{15}. The sublevels of 2S and $1F_z{}^3$ are the corresponding subshells of the Si_{15} TR. Overall, orbital interactions further indicate that the anti-bonding MOs of Mn_2 dimer enjoy stabilizing overlaps with different sublevels of Si_{15} TR, while the bonding MOs of Mn_2 are reinforced. Both effects thus induce an extra stability for the tubular cluster **I**.

Conclusions

The novel result emerges from this theoretical study is that we have found for the first time the smallest triple ring structure of silicon cluster, which is stabilized following doping of two Mn atoms. $Mn_2@Si_{15}$ **I** is a tubular structure in which Mn_2 dimer is inserted along the main axis of a (3×5) Si_{15} anti-prism motif. The Mn dopants connect with Si atoms of Si_{15} framework by single Si–Mn bonds while the Mn–Mn bond has a triple character. The effect of Mn_2 dimer on the enhanced stability of $Mn_2@Si_{15}$ is understood from orbital interactions in which the strong orbital overlaps of Mn_2 with Si_{15} entities not only stabilize anti-bonding MOs but also enhance the stability of bonding MOs, and thereby allow the emergence of a tubular silicon cluster. Thus it appears possible to make silicon tubes by using appropriate dopants.

Acknowledgements

MTN is indebted to the KU Leuven Research Council (GOA and IDO programs) for continuing support. NMT thanks KU Leuven for a postdoctoral fellowship. The authors are grateful to the Department of Science and Technology of Ho Chi Minh City, Vietnam for research grants.

Notes and references

1 W. L. Brown, R. R. Freeman, K. Raghavachari and M. Schluter, *Science*, 1987, **235**, 860.
2 E. C. Honea, A. Ogura, C. A. Murray, K. Raghavachari, W. O. Sprenger, M. F. Jarrold and W. L. Brown, *Nature*, 1993, **366**, 42.
3 G. Pacchioni and J. Koutecký, *J. Chem. Phys.*, 1986, **84**, 3301.

4 N. Veldeman, P. Gruene, A. Fielicke, P. Claes, V. T. Ngan, M. T. Nguyen and P. Lievens, in *Handbook of Nanophysics. Clusters and Fullerenes*, ed. K. D. Sattler, CRC Press, Boca Raton, Florida, USA, ch. 5, 2010.
5 O. Cheshnovsky, S. H. Yang, C. L. Pettiette, M. J. Craycraft, Y. Liu and R. E. Smalley, *Chem. Phys. Lett.*, 1987, **138**, 119.
6 C. B. Winstead, S. J. Paukstis and J. L. Gole, *Chem. Phys. Lett.*, 1995, **237**, 81.
7 U. Röthlisberger, W. Andreoni and M. Parrinello, *Phys. Rev. Lett.*, 1994, **72**, 665.
8 S. Li, R. J. Van Zee, W. Weltner and K. Raghvachari, *Chem. Phys. Lett.*, 1995, **243**, 275.
9 K. M. Ho, A. A. Shvartsburg, B. Pan, Z. Y. Lu, C. Z. Wang, J. G. Wacker, J. L Fye and W. L. Brown, *Nature*, 1998, **392**, 582.
10 A. A. Shvartsburg, B. Liu, M. F. Jarrold and K. M. Ho, *J. Chem. Phys.*, 2000, **112**, 4517.
11 X. Zhu and X. C. Zeng, *J. Chem. Phys.*, 2003, **118**, 3558.
12 W. Hellmann, R. G. Hennig, S. Goedecker, C. J. Umrigar, B. Delley and T. Lenosky, *Phys. Rev. B: Condens. Matter Mater. Phys.*, 2007, **75**, 085411.
13 D. Manzoor, S. Krishnamurty and S. Pal, *J. Phys. Chem. C*, 2014, **118**, 7501.
14 Z. M. Khakimov, P. L. Tereshchuk, N. T. Sulaymanov, F. T. Umarova and M. T. Swihart, *Phys. Rev. B: Condens. Matter Mater. Phys.*, 2005, **72**, 115335.
15 P. L. Tereshchuk, Z. M. Khakimov, F. T. Umarova and M. T. Swihart, *Phys. Rev. B: Condens. Matter Mater. Phys.*, 2007, **76**, 125418.
16 V. T. Ngan, K. Pierloot and M. T. Nguyen, *Phys. Chem. Chem. Phys.*, 2013, **15**, 5493.
17 Z. Liu, X. Wang, J. Cai and H. Zhu, *J. Phys. Chem. C*, 2015, **119**, 1517.
18 T. Iwasa and A. Nakajima, *J. Phys. Chem. C*, 2012, **116**, 14071.
19 S. M. Beck, *J. Chem. Phys.*, 1987, **87**, 4233.
20 V. T. Ngan, P. Gruene, P. Claes, E. Janssens, A. Fielicke, M. T. Nguyen and P. Lievens, *J. Am. Chem. Soc.*, 2010, **132**, 15589.
21 N. M. Tam, V. T. Ngan, J. de Haeck, S. Bhattacharyya, H. T. Le, E. Janssens, P. Lievens and M. T. Nguyen, *J. Chem. Phys.*, 2012, **136**, 024301.
22 V. T. Ngan and M. T. Nguyen, *J. Phys. Chem. A*, 2010, **114**, 7609.
23 N. M. Tam, T. B. Tai and M. T. Nguyen, *J. Phys. Chem. C*, 2012, **116**, 20086.
24 V. Kumar and Y. Kawazoe, *Phys. Rev. Lett.*, 2002, **88**, 235504.
25 M. B. Abreu, A. C. Reber and S. N. Khanna, *J. Phys. Chem. Lett.*, 2014, **5**, 3492.
26 J.-G. Han, R.-N. Zhao and Y. Duan, *J. Phys. Chem. A*, 2007, **111**, 2148.
27 W. Ji and C. Luo, *Int. J. Quantum Chem.*, 2012, **112**, 2525.
28 X. Huang, S.-J. Lu, X. Liang, Y. Su, L. Sai, Z.-G. Zhang, J. Zhao, H.-G. Xu and W. Zheng, *J. Phys. Chem. C*, 2015, **119**, 10987.
29 X. Huang, H.-G. Xu, S. Lu, Y. Su, R. B. King, J. Zhao and W. Zheng, *Nanoscale*, 2014, **6**, 14617.
30 M. J. Frisch, H. B. Schlegel, G. E. Scuseria, M. A. Robb, J. R. Cheeseman, J. A. Montgomery, T. Vreven, K. N. Kudin, J. C. Burant and J. Millam, *et al.*, *Gaussian 09 Revision: B.01*, Gaussian, Inc., Wallingford, CT, 2009.
31 J. M. Tao, J. P. Perdew, V. N. Staroverov and G. E. Scuseria, *Phys. Rev. Lett.*, 2003, **91**, 146401.
32 D. E. Woon and T. H. Dunning Jr, *J. Chem. Phys.*, 1993, **98**, 1358.
33 J. R. Li, G. H. Wang, C. H. Yao, Y. W. Mu, J. G. Wan and M. Han, *J. Chem. Phys.*, 2009, **130**, 164514.
34 K. Koyasu, M. Akutsu, M. Mitsui and A. Nakajima, *J. Am. Chem. Soc.*, 2005, **127**, 4998.
35 V. Chauhan, M. B. Abreu, A. C. Reber and S. N. Khanna, *Phys. Chem. Chem. Phys.*, 2015, **17**, 15718.
36 M. Kohout, F. R. Wanger and Y. Grin, *Int. J. Quantum Chem.*, 2006, **106**, 1499.
37 J. M. Goicoechea and J. E. McGrady, *Dalton Trans.*, 2015, **44**, 6755.
38 M. B. Abreu, A. C. Reber and S. N. Khanna, *J. Phys. Chem. Lett.*, 2014, **5**, 3492.
39 R. B. King, I. Silaghi-Dumitrescu and M. M. Uă, *Inorg. Chem.*, 2009, **48**, 8508.
40 B. Zhou, T. Kramer, A. L. Thompson, J. E. McGrady and J. M. Goicoechea, *Inorg. Chem.*, 2011, **50**, 8028.
41 T. B. Tai, H. M. T. Nguyen and M. T. Nguyen, *Chem. Phys. Lett.*, 2011, **502**, 187.
42 X. Huang, H.-G. Xu, S. Lu, Y. Su, R. B. King, J. Zhao and W. Zheng, *Nanoscale*, 2014, **6**, 14617.
43 E. N. Esenturk, J. Fettinger and B. Eichhorn, *J. Am. Chem. Soc.*, 2006, **128**, 9178.
44 M. M. Utą, D. Cioloboc and R. B. King, *J. Phys. Chem. A*, 2012, **116**, 9197.
45 P. Pyykko and N. Runeberg, *Angew. Chem., Int. Ed.*, 2002, **41**, 2174.
46 V. M. Medel, A. C. Reber, V. Chauhan, P. Sen, A. M. Köster, P. Calaminici and S. N. Khanna, *J. Am. Chem. Soc.*, 2014, **136**, 8229.
47 L. V. Duong, H. T. Pham, N. M. Tam and M. T. Nguyen, *Phys. Chem. Chem. Phys.*, 2014, **16**, 19470.
48 H. T. Pham, L. V. Duong and M. T. Nguyen, *J. Phys. Chem. C*, 2014, **118**, 24181.

